An extended siderophore suite from *Synechococcus* sp. PCC 7002 revealed by LC-ICPMS-ESIMS.

Rene M. Boiteau[a,b] and Daniel J. Repeta[a]

[a]Department of Marine Chemistry and Geochemistry, Woods Hole Oceanographic Institution, Woods Hole, MA 02543

[b]Department of Earth, Atmospheric and Planetary Sciences, Massachusetts Institute of Technology, Cambridge, MA 02139

Abstract

Siderophores are thought to play an important role in iron cycling in the ocean, but relatively few marine siderophores have been identified. Sensitive, high throughput methods hold promise for expediting the discovery and characterization of new siderophores produced by marine microbes. We developed a methodology for siderophore characterization that combines liquid chromatography (LC) inductively coupled plasma mass spectrometry (ICPMS) with high resolution electrospray ionization mass spectrometry (ESIMS). To demonstrate this approach, we investigated siderophore production by the marine cyanobacteria *Synechococcus* sp. PCC 7002. Three hydroxamate siderophores, synechobactin A-C, have been previously isolated and characterized from this strain. These compounds consist of an iron binding head group attached to a fatty acid side chain of variable length (C_{12}, C_{10}, and C_8 respectively). In this study, we detected six iron-containing compounds in *Synechococcus* sp. PCC 7002 media by LC-ICPMS. To identify the molecular ions of these siderophores, we aligned the chromatographic retention times of peaks from the LC-ICPMS chromatogram with features detected from LC-ESIMS spectra using an algorithm designed to recognize metal isotope patterns. Three of these compounds corresponded to synechobactins A (614 m/z), B (586m/z), and C (558m/z). The MS2 spectra of these compounds revealed diagnostic synechobactin fragmentation patterns which were used to confirm the identity of the three unknown compounds (600, 628, and 642 m/z) as new members of the synechobactin suite with side chain lengths of 11, 13, and 14 carbons. These results demonstrate the potential of combined LCMS techniques for the identification of novel iron-organic complexes.

Introduction

Iron availability can influence the biological productivity and ecosystem community composition of the ocean[1–4]. In oxic seawater, dissolved iron (III) rapidly forms insoluble oxyhydroxides and precipitates from solution[5]. This poses a challenge to microbes that require iron for photosynthesis, nitrogen fixation, respiration, protection against oxidative stress, and other essential biological processes. In regions where available iron is scarce, microbes may gain a competitive advantage by producing siderophores; biomolecules that strongly and specifically complex iron in a form that can be recovered using dedicated membrane transporters[6,7].

Isolating and identifying siderophores is important for understanding the competition for iron in regions of the ocean where iron scarcity exerts a selective pressure on the microbial community. Indeed, siderophores appear to be present at low concentrations in seawater collected from open ocean sites[8], and metagenomic analysis has suggested that siderophore production and uptake in the ocean may be common[9–12]. Some siderophores have been discovered in the extracts of a number of marine bacteria grown in laboratory cultures[13]. However their characterization in marine environmental samples remains a challenge due to their low concentrations. Of the known marine siderophores, many are amphiphilic, consisting of a polar, iron-binding head group and a nonpolar fatty acid tail[14–19], which may allow the siderophore to be tethered to the outer cell membrane or form micelles in an environment where free siderophores might otherwise diffuse away too quickly to facilitate iron uptake[20,21]. It is common for amphiphilic siderophores to occur as homologous series with fatty acid tails that differ by CH_2, such that a single bacteria may produce a suite of structurally related siderophores.

Liquid chromatography (LC) coupled to mass spectrometry offers a sensitive, high throughput means of detecting and characterizing siderophores. Two complementary methods have been used to detect organic-metal complexes: inductively coupled plasma mass spectrometry (ICPMS) and electrospray ionization mass spectrometry (ESIMS)[22–26]. In the case of ICPMS, as the metal complexes elute from the chromatography column, the metal is atomized and detected directly as the elemental ion. This is a convenient method for sensitively detecting metal complexes and estimating their abundances in biological and environmental samples[8,27–30]. However, ICPMS provides no information on the structure of the organic complex. Electrospray ionization mass spectrometry (ESIMS) can be used to detect isotopologues of the intact metal complexes[31–35]. For metals such as iron that have multiple isotopes, computer algorithms can search LC-ESIMS mass spectra and identify features that match a metal's characteristic isotope pattern[33–35]. Furthermore, ESI instruments capable of generating MS2 spectra of the parent ion can reveal diagnostic fragmentation patterns that facilitate compound identification. However, it is difficult to quantify organic-metal complexes using ESIMS, and search algorithms often miss isotopologues that occur in low abundance or report false positives due to isobaric interferences from co-eluting compounds[36].

We developed a methodology that combines both LCMS techniques and used it to investigate the production of siderophores by *Synechococcus* sp. PCC 7002 (Fig. 1). The metabolites produced by this fast growing model marine cyanobacteria have been the focus of numerous studies[37–42]. *Synechococcus* sp. PCC 7002 is known to produce a suite of three siderophores known as synechobactins A, B and C[43–45]. Synechobactins consist of a citrate head group attached to two 1,3-diaminopropane moieties. The terminal amines of the diaminopropane moieties are hydroxylated and one is linked to acetic acid while the other is linked to a fatty acid (Fig. 2). Synechobactins A-C differ by the carbon number of their fatty acid chains, with synechobactin A having octanoic acid (C_8), B having decanoic acid (C_{10}), and C having dodecanoic acid (C_{12})[45]. Additional iron complexes were later detected in the media of *Synechococcus* sp. PCC 7002 with LC-ICPMS[29]. Here we report the improved separation of *Synechococcus* sp. PCC 7002

siderophores and the use of an isotope matching algorithm to assign parent ion masses to three previously undescribed complexes. By comparing the MS2 fragmentation spectra of known synechobactins to the unknown complexes, we were able to identify them as new members of the synechobactin family of siderophores.

Experimental

Materials and reagents

Ultrahigh purity water (18.2 MΩ cm), and LCMS grade methanol (MeOH), ammonium formate, and formic acid (Optima, Fisher scientific) were used in this study. The methanol was further purified by sub-boiling-point distillation in a polytetrafluoroethylene (PTFE) still to reduce Fe contamination[29]. Nutrient salts and vitamins for culture media were obtained from Sigma Aldrich. Polycarbonate plastic bottles used for culturing and PTFE vials for sample storage were soaked overnight in 0.1% detergent (Citranox), rinsed 5x with H_2O, and then soaked in 1 N hydrochloric acid (J.T. Baker) for 2 days followed by a final 5x rinse with H_2O. PTFE and platinized silicone tubing (Cole Parmer) and tube adapters (Visiprep, Sigma Aldrich) used for solid phase extraction were cleaned by rinsing with 1 N HCl through the tubing for 12 hrs followed by rinsing with H_2O for another 12 hours using a peristaltic pump (Cole Parmer). All samples for LCMS analysis were placed in certified 2 mL amber glass autosampler vials or 250 μL vial inserts (Agilent).

Synechococcus sp. PCC 7002 culture

Cultures of *Synechococcus* sp. PCC 7002 were grown in polycarbonate bottles in continuous light at 23°C. A 10 mL inoculum was used to inoculate 500mL of sterile SN medium[46] containing only 50 nM $FeCl_3*6H_2O$ plus 1 μg/L cyanocobalamin. After seven days of growth, the culture media was centrifuged to remove cells, filtered (0.2 μm polyethersulfone sterivex, Millipore), and pumped through an ENV+ resin column (1 g, 6 mL, Biotage) at a flow rate of 10 mL/min. A 500 mL volume of sterile media was processed as a procedural blank to monitor contamination. The columns were rinsed with H_2O to remove salts and eluted with 6 mL of distilled MeOH into PTFE vials. This organic extract was concentrated to 0.5 mL by evaporation under a stream of nitrogen gas and stored in the dark at -20°C until analysis by LC-MS. Effort was made to minimize exposure of the sample to light and avoid photodegradation.

Liquid chromatography

Organic extracts were separated using an Agilent 1260 series bioinert high pressure chromatography pump and autosampler fitted with a C18 column (Kinetex 2.1x100mm, 1.7 μm particle size) and polyetheretherketone (PEEK) tubing and connectors. The mobile phase consisted of (A) 5 mM aqueous ammonium formate or 0.1% formic acid in H_2O (B) 5 mM ammonium formate or 0.1% formic acid in distilled MeOH. Optimal separation and electrospray ionization were achieved using ammonium formate buffer and a 30 minute solvent gradient from 5% to 100% B followed by a 10 minute isocratic

elution in 100% B at a flow rate of 100 µL/min. A post column PEEK flow splitter directed 50% of the flow into the ICP-MS or ESI-MS. Reducing the flow entering the ICP-MS to 50 µL/min eliminated the need for post-column desolvation, even when eluting with 100% organic phase. On the same column, chromatographic retention times were reproducible within 0.1 min over several months of analysis.

LC-ICPMS conditions

The flow of the LC column was coupled directly to a quadrupole ICPMS (Thermo ICAPq) using a teflon STD micronebulizer (ESI) and a cyclonic spray chamber cooled to 0°C. Oxygen gas was introduced to the plasma at 25 mL/min to combust organic solvents and buffers to CO_2 thereby preventing the formation of reduced carbon deposits that would otherwise accumulate on the cones. The ICPMS was equipped with platinum sampler and skimmer cones, and was tuned each day using an automated tuning feature and the 'Tune B' solution purchased from Thermo Scientific. ^{54}Fe, ^{56}Fe, ^{57}Fe, and ^{59}Co were monitored with an integration time of 0.05 seconds each. The instrument was run in KED mode with a He collision gas introduced at a rate of 4.2 mL/min to minimize ArO^+ interferences on ^{56}Fe.

LC-ESIMS conditions

For LC-ESIMS analysis, the flow from the LC was coupled to a Thermo Scientific Orbitrap Fusion mass spectrometer equipped with a heated electrospray ionization source. ESI source parameters were set to a capillary voltage of 3500 V, sheath, auxiliary and sweep gas flow rates of 12, 6, and 2 (arbitrary units), and ion transfer tube and vaporizer temperatures of 300°C and 75°C. MS1 scans were collected in high resolution (450K) positive and negative mode. High energy collision induced dissociation (HCD) MS2 spectra for the most abundant compounds in each orbitrap scan were collected simultaneously on the ion trap mass analyzer. Ions were trapped using quadrupole isolation of a ± 2 m/z mass window and were then fragmented using an HCD collision energy of 35%. For the six iron containing compounds investigated in this study, targeted high resolution MS2 spectra were collected with the orbitrap mass analyzer during a second analytical run to obtain accurate fragment masses.

Data processing

The LC-ESIMS data was converted to mzXML file format (MSconvert, proteowizard) and iron isotopologue features were identified using a data-mining algorithm (script written in R using xcmsRaw class[47]). This algorithm searches through each ms scan and compiles a list of peak sets (retention time, masses, and intensities) that fit a specified isotope pattern. Both low tolerance and high tolerance (described below) peak ratio filters were used. The compiled peak sets are then binned by mass in 0.01 m/z increments. Two criteria are used to automatically remove mass sets that result from instrumental noise rather than chromatographic peaks: (1) Mass sets that do not appear at least twice within a 10 second interval are discarded. (2) Mass sets that are found in 8 or more 30 second intervals are discarded if they do not contain any points above the intensity baseline. The

baseline is calculated based on the maximum intensity points from each 30 second time interval. The highest 25% of intensities are discarded, and the baseline is calculated as 3x the standard deviation plus the mean of the remaining values.

The resulting mass list was manually curated by inspecting the extracted ion chromatograms (EICs) of the putative isotopologues. A constant time offset was applied to the LC-ESIMS chromatogram in order to align the retention time of the cyanocobalamin $[M+H]^{2+}$ peak (EIC of m/z = 678) with the cyanocobalamin ^{59}Co peak at 20.7 min in the LC-ICPMS chromatogram. Iron-containing ions were considered valid if peaks in the EICs: (1) Have the same retention time and peak shape compared to each other when the intensities are scaled relative to the expected isotope ratio. (2) Have the same retention time as the associated peak in the LC-ICPMS spectrum.

Results and discussion

LC-ICP-MS

Tandem LC-ICPMS enables rapid detection of metal organic complexes. Over the course of the chromatographic separation, siderophores elute from the column and enter the plasma where the iron is atomized, ionized, and detected by the mass spectrometer as $^{56}Fe^{+}$. The chromatogram that results from this analysis indicates the retention time and abundance of each compound that contains iron.

LC-ICPMS was used to detect iron-binding compounds extracted from *Synechoccocus* sp. PCC 7002 culture (Fig. 3a). Chromatographic conditions were optimized to achieve baseline resolution of the compounds which appear as six distinct peaks of iron, with characteristic retention times of 29.4, 33.9, 35.8, 37.1, 38.5 and 39.6 minutes. This separation was achieved using a 30-minute gradient from 0-100% methanol using a 5 mM aqueous ammonium formate buffer.

LC-ESIMS

While ICPMS provides information on the quantity and number of different ligands in the samples along with their retention times, ESIMS provides complimentary information on the parent ion mass and fragmentation pattern. Using the same chromatography as described above, the *Synechococcus* media extract was analyzed by LC-ESIMS. As a soft ionization technique, ESIMS measures the mass of the intact metal-ligand complexes.

Samples were analyzed in both positive and negative ionization modes, with either 0.1% formic acid or 5 mM ammonium formate as a mobile phase buffer. For the previously characterized siderophores (synechobactins A, B, and C), the use of 5 mM ammonium formate in positive mode resulted in the greatest parent ion signal intensity. The apo (metal-free) form of the siderophore was also detected under these conditions, although the intensity was <2% relative to the iron-bound form. When 0.1% formic acid was used in the mobile phase, the parent ion signal decreased by a factor of 10 and the apo form intensity was 8-11% relative to the iron-bound form. While the intensity ratio between a

ligand and its complex in ESI MS spectra does not necessarily reflect concentration ratio as the two species may ionize differently in an ESI source, these results demonstrate that ammonium formate is a preferred buffer for detecting iron-bound hydroxamate siderophores such as synechobactins.

To determine the masses of the three major unknown iron containing compounds, an R based algorithm was used to extract mass spectral features that matched the natural abundance pattern of iron stable isotopes. Results were manually curated to determine which matches aligned with one of the six iron peaks detected by LC-ICPMS (Fig. 3). The choice of isotope pattern criteria balances flexibility and specificity. Ideally, the selection criteria are flexible enough to account for imprecision in the instrumental measurement but specific enough to exclude other common isotope patterns and to reduce the risk of false positives that result from co-eluting ions or from instrumental noise that coincidentally match the specified isotope pattern.

The algorithm used in this study searched each spectral scan for pairs of peaks with a mass difference of 1.995 m/z and a light/heavy intensity ratio of 0.06, corresponding to isotopologues containing ^{54}Fe and ^{56}Fe respectively. A mass window of ± 3 mDa was used to account for uncertainty in the accuracy of the orbitrap analyzer at 450,000 mass resolution. Since the uncertainty in the isotopologue intensity ratio depends on signal intensity, detecting low abundance isotope pairs requires a larger range in the intensity ratio criteria than is required for more abundant compounds. When a narrow ratio window (0.06 ± 0.015) was used, 40 isotope pairs were identified by the algorithm and 17 of these peaks passed the manual curation step. Using a wide ratio window (0.06 ± 0.036), 92 isotope sets were initially identified, and 29 passed the manual curation step. The most abundant isotope pair found at each retention time was assigned as the parent ion (Fig. 3, Table 1). Other peak pairs corresponded to ^{13}C isotopologues as well as adducts with other abundant coeluting compounds (a complete list is included in the supplementary information, Fig. SI-1, Table SI-1).

MS2 Fragmentation

MS2 fragmentation patterns were used to structurally characterize the six synechobactins detected in this study (Fig. 4). Once the parent ion masses were assigned, the sample was reanalyzed by LC-ESIMS for targeted high resolution MS2 analysis. An isolation window of ±2 m/z was used to retain the iron isotope patterns of fragments that contain iron.

First, the characteristic fragmentation patterns of synechobactins A, B, and C (m/z 614.261, 586.23, and 558.198) were determined. Structurally, synechobactins consists of an iron binding head group composed of citrate and two aminopropane moieties linked to a fatty acid or acetic acid. Most of the major fragments that were observed for the known synechobactins retain iron (based on the appearance of ions corresponding to the ^{54}Fe and ^{56}Fe isotopologues). The MS2 analysis of all three synechobactins displayed a major fragment with neutral losses of 156.006 [$-C_6H_4O_5$], corresponding to cleavage at the amide linkage and loss of citrate (Fig. 5a). This fragmentation pattern is consistent with

those of other citrate and hydroxamate based siderophores[48–50]. Other major neutral mass losses correspond to fragmentation within the citrate head group including 46.006 [-CH_2O_2], 113.996 [-$C_4H_2O_4$], and 130.027 [-$C_5H_6O_4$]. Several additional fragments indicate head group cleavages that result in the loss of one of the hydroxamate groups (Fig. 5b). For synechobactin A, for instance, these fragments occur in pairs that differ by $C_{10}H_{20}$ (140.157 m/z), corresponding to the loss of the long fatty acid hydroxamate side chain (including fragments at 206.035, 270.030, 288.040, 298.025, Fig. 4d) and the acetohydroxamate respectively (fragments at 346.191, 410.186, 428.198, and 438.181, Fig. 4d). MS2 spectra of the positive apo (iron free) ion of synechobactin A-B and the negative iron-bound ion of synechobactin A were also measured (supplementary information, Fig. SI-2).

The fragmentation patterns of synechobactins A-C help in the interpretation of MS2 spectra of the three uncharacterized siderophores. The mass difference between the unknown compounds and synechobactins A-C correspond to the addition or loss of $(CH_2)_n$ ($\Delta m/z = n*14$). All three uncharacterized siderophores exhibit neutral losses that are characteristic of fragmentation of a citrate head group including 46.006 [-CH_2O_2], 113.996 [-$C_4H_2O_4$], 130.027 [-$C_5H_6O_4$], and 156.006 [-$C_6H_4O_5$]. They also contain the 206.035, 270.030, 288.040, and 298.025 fragments that are attributed to cleavage across the citrate head group that retains the acetohydroxamate group. Thus, these new compounds vary by the length of the fatty acid side chain, and correspond to the C_{13}, C_{15}, and C_{16} synechobactins.

The MS2 spectra of the low abundance siderophores with m/z of 600.245 and 628.276 contain additional fragments from coeluting compounds (red masses, Fig. 4). By obtaining off-peak MS2 scans from the interfering parent ions, we were able to identify the masses that arise from the interfering ion rather than the siderophore (supplementary information, Fig. SI-3).

Connection to synechobactin biosynthesis

The six major compounds detected by LC-ICPMS were all identified as homologues of synechobactin A. A search for ions in the LC-ESIMS spectra that correspond to other synechobactin homologues revealed low intensity peaks that potentially correspond to C_9-synechobactin and C_{16}-synechobactin, although the ^{54}Fe isotopologues for both were below detection (supplementary information, Fig. SI-4). These results reveal that *Synechococcus* sp. PCC 7002 is capable of incorporating a wide range of fatty acids into the hydroxamate side chain of synechobactin. There appears to be a preference for an even number of carbons over odd carbon numbers. Additional synechobactins with longer hydrophobic side chains may have been present in the sample, but were not recovered from the extraction column by the methanol wash.

Such a wide range of siderophores produced by *Synechococcus* sp. PCC 7002 suggests substrate flexibility for the enzymes involved in synechobactin biosynthesis. The operon responsible for synechobactin synthesis (SYNPCC7002_G0019-G0024) is located on a plasmid that is largely dedicated to the synthesis, uptake, and processing of these

compounds, and these genes are upregulated in low iron conditions[51]. Synechobactin synthesis appears to be similar to the synthesis of rhizobactin, which is structurally equivalent to synechobactin B (C_{10}) with a trans double bond between carbons 2,3 of the fatty acid side chain (Fig. 2). The production of rhizobactin is thought to involve the synthesis of schizokinen, which contains two acetohydroxamates[52], followed by the replacement of one acetic acid with 2-decenoic acid[53]. It also is possible that *Synecoccoccus* sp. PCC 7002 uses schizokinen as an intermediate in synechobactin synthesis. Indeed, in a culture of *Synechococcus* sp. PCC 7002 that was harvested at an earlier growth phase, an additional chromatographic ^{56}Fe peak was observed[29] with m/z 474 that corresponds to schizokinen (supplementary information Fig. SI-5). A putative lipase that is encoded at the end of the synechobactin biosynthesis operon (SYNPCC7002_G0018) may be responsible for non-specifically catalyzing the attachment of the fatty acid side chain to the synechobactin precursor. A better understanding of the metabolic pathways involved in catalyzing this reaction will help reveal how amphiphilic marine siderophores are produced, shed light on how this functionality evolved, and will improve our ability to search for amphiphilic siderophore biosynthetic potential in marine genomic/metagenomic libraries.

Conclusions

The methodology described here provides a means to confidently detect and determine the masses and MS2 spectra of even minor siderophores in a biological extract with no prior knowledge of the siderophores produced in a culture. Common siderophore functional groups can have diagnostic fragmentation patterns that facilitate structural characterization of new siderophores, as illustrated in this study with the citrate head group fragmentation of the synechobactins. Using this approach, we were able to characterize three new synechobactins, and provide preliminary evidence for two additional homologues that may be present at very low concentrations. As MS2 libraries of known siderophores grow, our ability to characterize new siderophores based on high resolution mass spectrometry analysis will improve.

The combination of LC-ICPMS and LC-ESIMS has the potential to increase the pace and depth of siderophore discovery. Looking ahead, this work represents a step towards the eventual goal of detecting and characterizing metal-binding organic compounds directly in environmental samples where they impact ecosystems and trace metal cycling. Organic complexation is thought to largely control iron solubility and bioavailability in the ocean[54–56], and understanding the speciation of iron is critical for forecasting ecosystem changes in low iron regions of the ocean[57–59]. The challenge of characterizing these marine iron binding molecules (including siderophores[8,60], heme[61,62], polysaccharides[63,64], and humic substances[65–70]) lies in their low concentrations (often sub-picomolar for a specific compound) within a very complex organic matrix. Methods such as the one described in this study have the potential to address these challenges and reveal the structural diversity of metal organic ligands in environmental samples.

Acknowledgements

We would like to thank Matt McIlvin for his assistance with the orbitrap mass spectrometer, John Waterbury and Athena Archer for supplying the *Synechococcus* sp. PCC 7002 strain, and two anonymous reviewers for their constructive comments. This work was supported by the National Science Foundation program in Chemical Oceanography (OCE-1356747), and by the National Science Foundation Science and Technology Center for Microbial Oceanography Research and Education (C-MORE; DBI-0424599).

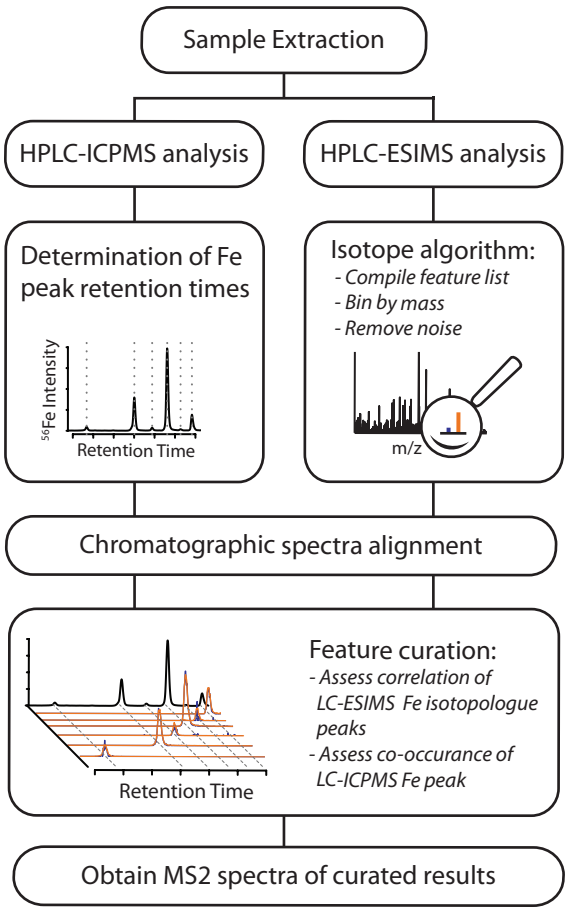

Figure 1: Workflow for unknown iron compound identification by combined LC-ICPMS-ESIMS.

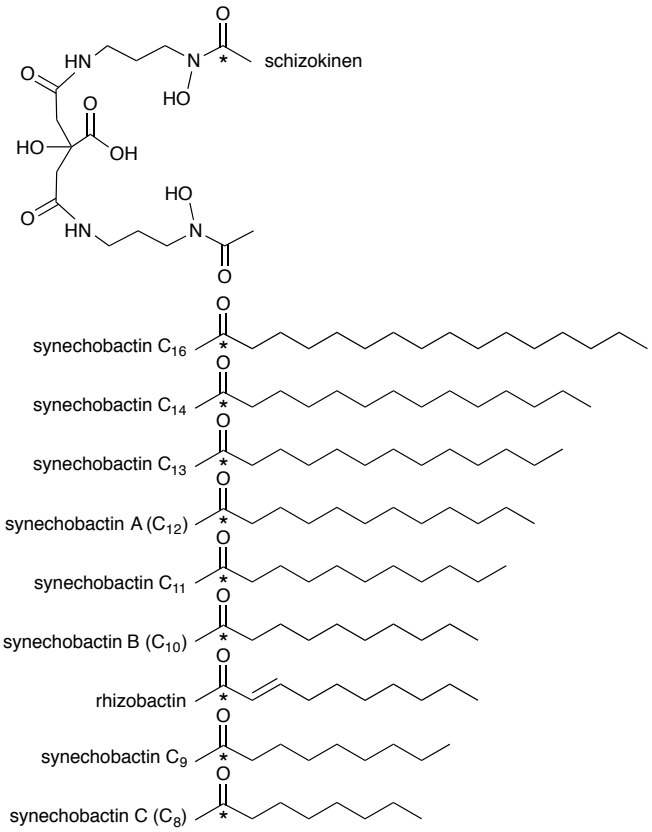

Figure 2: Chemical structure of the synechobactins and related compounds. The hydroxamate side chain (indicated by *) differentiates these compounds.

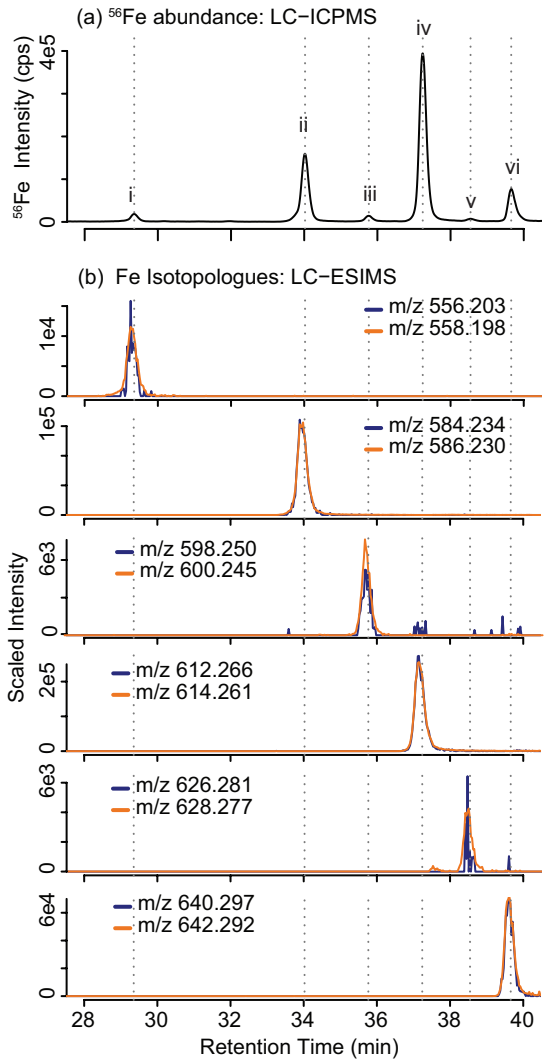

Figure 3: LC-MS chromatograms of *Synechoccoccus* sp. PCC 7002 media extract. (a) ^{56}Fe LC-ICPMS chromatogram. The six labeled peaks correspond to siderophores produced by *Synechococcus* sp. PCC 7002 in this experiment (b) extracted ion chromatograms from positive mode LC-ESIMS runs. Blue lines correspond to the light iron isotopologue [M+$^{54}Fe^{3+}$-2H^{+}] that were identified by the isotope algorithm, and orange lines correspond to the heavy iron isotopologue [M+$^{56}Fe^{3+}$-2H^{+}]. The intensity of the heavy iron isotopologue has been scaled by the natural abundance ratio of ^{56}Fe/^{54}Fe (divided by 15.7) so that the isotopologues overlap.

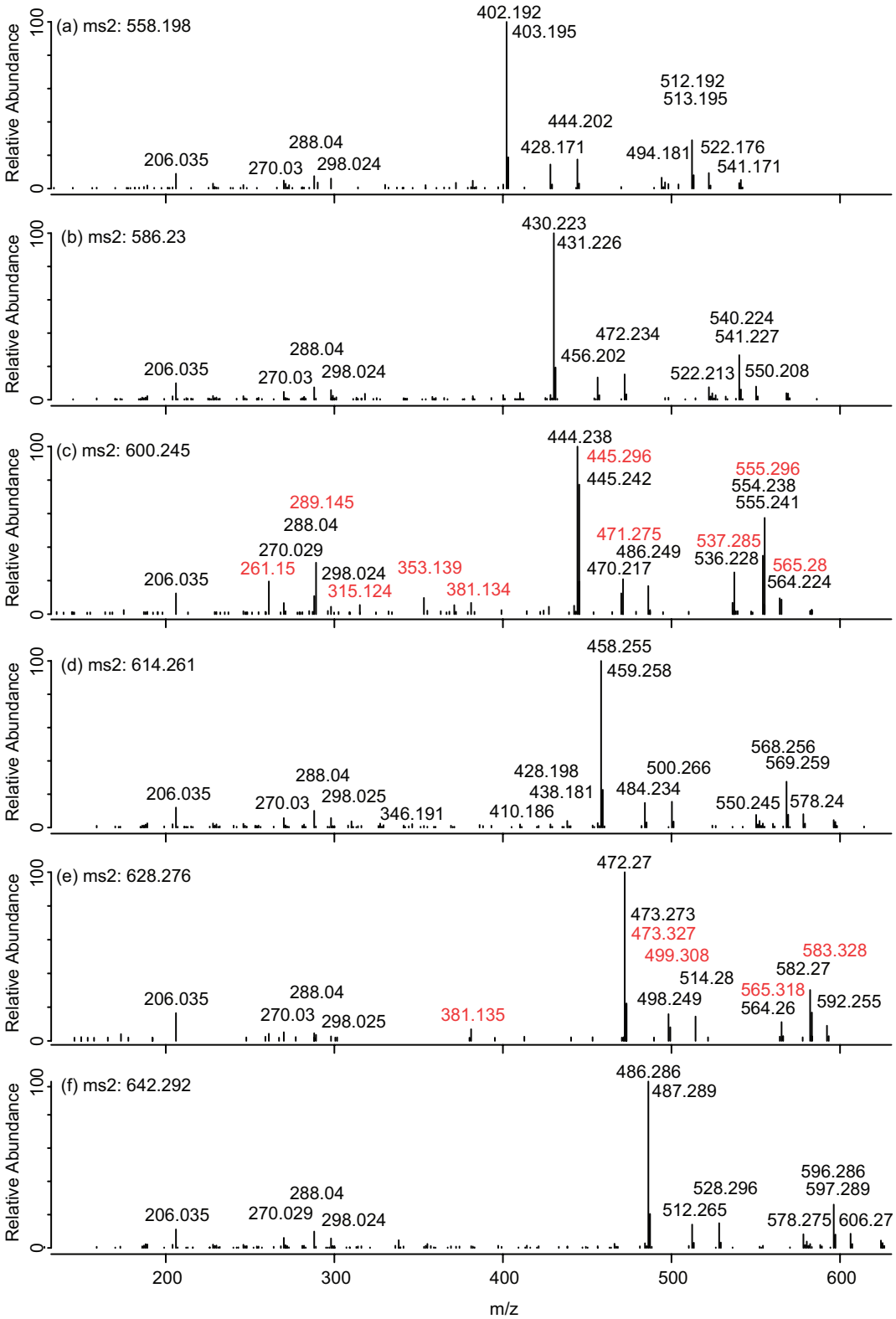

Figure 4: Positive mode MS2 spectra of the six identified Fe containing compounds. (a) C_8-Synechobactin, (b) C_{10}-synechobactin, (c) C_{11}-synechobactin (d) C_{12}-synechobactin (e) C_{13}-synechobactin (f) C_{14}-synechobactin. Red labels correspond to interferences from a coeluting ion (see supplementary information Figure 2).

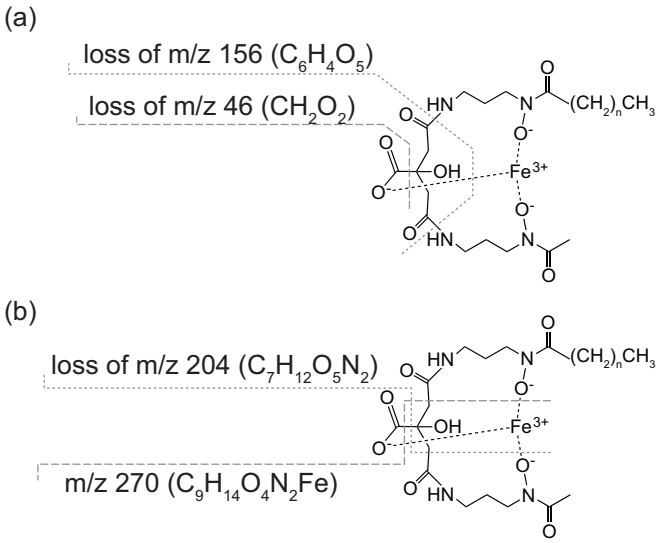

Figure 5: Characteristic fragmentation patterns of Fe-synechobactins. (a) Major fragmentations that result in the loss of the citrate head group. (b) Example of fragment pair that results in the symmetric loss of the short and long hydroxamate side chains.

Table 1: Siderophores from *Synechococcus* sp. PCC 7002

Monoisotopic m/z (^{56}Fe form)	Retention Time (min)	Parent ion formula	Compound I.D.
558.198	29.4	$C_{22}H_{38}O_9N_4Fe^+$	synechobactin C (C_8)*
572.214	31.9	$C_{23}H_{40}O_9N_4Fe^+$	synechobactin C_9†
586.230	33.9	$C_{24}H_{42}O_9N_4Fe^+$	synechobactin B (C_{10})*
600.245	35.8	$C_{25}H_{44}O_9N_4Fe^+$	synechobactin C_{11}
614.261	37.1	$C_{26}H_{46}O_9N_4Fe^+$	synechobactin A (C_{12})*
628.276	38.5	$C_{27}H_{48}O_9N_4Fe^+$	synechobactin C_{13}
642.292	39.6	$C_{28}H_{50}O_9N_4Fe^+$	synechobactin C_{14}
670.324	41.8	$C_{30}H_{54}O_9N_4Fe^+$	synechobactin C_{16}†

*Previously described by *Ito and Butler*, 2005

†Putative ID based on detection of ^{56}Fe monoisotopic mass. ^{54}Fe isotopologue and MS2 peaks were below detection limit.

References

1. W. G. Sunda, *Front. Microbiol.*, 2012, **3**, 204.

2. J. K. Moore and S. C. Doney, *Global Biogeochem. Cycles*, 2007, **21**.

3. F. M. M. Morel, A. J. Milligan, and M. A. Saito, *Treatise Geochemistry, Vol. 6*, 2003.

4. H. De Baar, P. Boyd, K. Coale, and M. Landry, *J. Geophys. Res*, 2005, **110**, 1–24.

5. X. Liu and F. Millero, *Mar. Chem.*, 2002, **77**, 43–54.

6. V. Braun and H. Killmann, *Trends Biochem. Sci.*, 1999, **24**, 104–9.

7. C. Wandersman and P. Delepelaire, *Annu. Rev. Microbiol.*, 2004, **58**, 611–47.

8. E. Mawji, M. Gledhill, J. A. Milton, G. A. Tarran, S. Ussher, A. Thompson, G. A. Wolff, P. J. Worsfold, and E. P. Achterberg, *Environ. Sci. Technol.*, 2008, **42**, 8675–80.

9. E. Toulza, A. Tagliabue, S. Blain, and G. Piganeau, *PLoS One*, 2012, **7**, e30931.

10. B. M. Hopkinson and K. A. Barbeau, *Environ. Microbiol.*, 2012, **14**, 114–28.

11. D. K. Desai, F. D. Desai, and J. La Roche, *Front. Microbiol.*, 2012, **3**, 362.

12. M. Li, B. M. Toner, B. J. Baker, J. A. Breier, C. S. Sheik, and G. J. Dick, *Nat. Commun.*, 2014, **5**, 3192.

13. A. Butler, *Biometals*, 2005, **18**, 369–374.

14. J. M. Vraspir, P. D. Holt, and A. Butler, *Biometals*, 2011, **24**, 85–92.

15. J. S. Martinez, J. N. Carter-Franklin, E. L. Mann, J. D. Martin, M. G. Haygood, and A. Butler, *Proc. Natl. Acad. Sci. U. S. A.*, 2003, **100**, 3754–9.

16. V. V Homann, M. Sandy, J. A. Tincu, A. S. Templeton, B. M. Tebo, and A. Butler, *J. Nat. Prod.*, 2009, **72**, 884–8.

17. J. M. Gauglitz and A. Butler, *J. Biol. Inorg. Chem.*, 2013, **18**, 489–97.

18. J. D. Martin, Y. Ito, V. V Homann, M. G. Haygood, and A. Butler, *J. Biol. Inorg. Chem.*, 2006, **11**, 633–41.

19. J. S. Martinez and A. Butler, *J. Inorg. Biochem.*, 2007, **101**, 1692–1698.

20. J. Martinez, G. Zhang, P. Holt, and H. Jung, *Science*, 2000, **287**, 1245–1247.

21. G. Xu, J. S. Martinez, J. T. Groves, and A. Butler, *J. Am. Chem. Soc.*, 2002, **124**, 13408–15.

22. R. Lobiński, D. Schaumlöffel, and J. Szpunar, *Mass Spectrom. Rev.*, 2006, **25**, 255–89.

23. S. Mounicou, J. Szpunar, and R. Lobinski, *Chem. Soc. Rev.*, 2009, **38**, 1119–38.

24. Z. Pedrero, L. Ouerdane, S. Mounicou, R. Lobinski, M. Monperrus, and D. Amouroux, *Metallomics*, 2012, **4**, 473–9.

25. T. Grevenstuk, P. Flis, L. Ouerdane, R. Lobinski, and A. Romano, *Metallomics*, 2013, **5**, 1285–93.

26. L. Grillet, L. Ouerdane, P. Flis, M. T. T. Hoang, M. Isaure, R. Lobinski, C. Curie, and S. Mari, *J. Biol. Chem.*, 2014, **289**, 2515–25.

27. D. Pröfrock and A. Prange, *Appl. Spectrosc.*, 2012, **66**, 843–68.

28. O. J. Lechtenfeld, G. Kattner, R. Flerus, S. L. McCallister, P. Schmitt-Kopplin, and B. P. Koch, *Geochim. Cosmochim. Acta*, 2014, **126**, 321–337.

29. R. M. Boiteau, J. N. Fitzsimmons, D. J. Repeta, and E. A. Boyle, *Anal. Chem.*, 2013, **85**, 4357–62.

30. R. Clough, C. F. Harrington, S. J. Hill, Y. Madrid, and J. F. Tyson, *J. Anal. At. Spectrom.*, 2014, **29**, 1158.

31. I. Velasquez, B. L. Nunn, E. Ibisanmi, D. R. Goodlett, K. A. Hunter, and S. G. Sander, *Mar. Chem.*, 2011, **126**, 97–107.

32. H. Waska, A. Koschinsky, M. J. Ruiz Chancho, and T. Dittmar, *Mar. Chem.*, 2014, DOI: 10.1016/j.marchem.2014.10.001.

33. S. M. Lehner, L. Atanasova, N. K. N. Neumann, R. Krska, M. Lemmens, I. S. Druzhinina, and R. Schuhmacher, *Appl. Environ. Microbiol.*, 2013, **79**, 18–31.

34. M. Deicke, J. F. Mohr, J.P. Bellenger, and T. Wichard, *Analyst*, 2014, DOI: 10.1039/c4an01461h.

35. O. Baars, F. M. M. Morel, and D. H. Perlman, *Anal. Chem.*, 2014, DOI: 10.1021/ac503000e.

36. M. J. Keith-Roach, *Anal. Chim. Acta*, 2010, **678**, 140–8.

37. R. Baran, B. P. Bowen, N. J. Bouskill, E. L. Brodie, S. M. Yannone, and T. R. Northen, *Anal. Chem.*, 2010, **82**, 9034–9042.

38. R. Baran, B. P. Bowen, and T. R. Northen, *Mol. Biosyst.*, 2011, **7**, 3200–6.

39. R. Baran, N. N. Ivanova, N. Jose, F. Garcia-Pichel, N. C. Kyrpides, M. Gugger, and T. R. Northen, *Mar. Drugs*, 2013, **11**, 3617–31.

40. I. Lanekoff, O. Geydebrekht, G. E. Pinchuk, A. E. Konopka, and J. Laskin, *Analyst*, 2013, **138**, 1971–8.

41. N. Bennette, J. Eng, and G. Dismukes, *Anal. Chem.*, 2011, **83**, 3808–16.

42. K. McNeely, Y. Xu, N. Bennette, D. a Bryant, and G. C. Dismukes, *Appl. Environ. Microbiol.*, 2010, **76**, 5032–8.

43. C. Trick and S. Wilhelm, *Mar. Chem.*, 1995, **50**, 207–217.

44. S. Wilhelm and D. Maxwell, *Limnol. Oceanogr.*, 1996, **41**, 89–97.

45. Y. Ito and A. Butler, *Limnol. Oceanogr.*, 2005, **50**, 1918–1923.

46. J. Waterbury, S. Watson, F. Valois, and D. Franks, *Can Bull Fish Aquat Sci*, 1986, **214**, 71.

47. C. A. Smith, E. J. Want, G. O'Maille, R. Abagyan, and G. Siuzdak, *Anal. Chem.*, 2006, **78**, 779–87.

48. M. Gledhill, *Analyst*, 2001, **126**, 1359–1362.

49. E. Mawji, M. Gledhill, P. J. Worsfold, and E. P. Achterberg, *Rapid Commun. Mass Spectrom.*, 2008, 2195–2202.

50. J. M. Gauglitz, H. Zhou, and A. Butler, *J. Inorg. Biochem.*, 2012, **107**, 90–5.

51. M. Ludwig and D. A. Bryant, *Front. Microbiol.*, 2012, **3**, 145.

52. K. B. Mullis, J. R. Pollack, and J. B. Neilands, *Biochemistry*, 1971, **10**, 4894–4898.

53. D. Lynch, J. O'Brien, T. Welch, P. Clarke, P. O. Cuív, J. H. Crosa, and M. O'Connell, *J. Bacteriol.*, 2001, **183**, 2576–85.

54. K. A. Hunter and P. W. Boyd, *Environ. Chem.*, 2007, **4**, 221.

55. M. Gledhill and K. N. Buck, *Front. Microbiol.*, 2012, **3**, 1–17.

56. S. M. Kraemer, O. W. Duckworth, J. M. Harrington, and W. D. C. Schenkeveld, *Aquat. Geochemistry*, 2014, DOI: 10.1007/s10498-014-9246-7.

57. A. Tagliabue, L. Bopp, O. Aumont, and K. R. Arrigo, *Global Biogeochem. Cycles*, 2009, **23**.

58. A. Tagliabue and C. Völker, *Biogeosciences*, 2011, **8**, 3025–3039.

59. D. Shi, Y. Xu, B. M. Hopkinson, and F. M. M. Morel, *Science*, 2010, **327**, 676–9.

60. E. Mawji, M. Gledhill, J. A. Milton, M. V. Zubkov, A. Thompson, G. A. Wolff, and E. P. Achterberg, *Mar. Chem.*, 2011, **124**, 90–99.

61. S. L. Hogle, K. A. Barbeau, and M. Gledhill, *Metallomics*, 2014, **6**, 1107–20.

62. M. Gledhill, *Anal. Chim. Acta*, 2014, **841**, 33–43.

63. C. S. Hassler, V. Schoemann, C. M. Nichols, E. C. V. Butler, and P. W. Boyd, *Proc. Natl. Acad. Sci.*, 2011, **108**, 1076–1081.

64. C. S. Hassler, L. Norman, C. A. Mancuso Nichols, L. A. Clementson, C. Robinson, V. Schoemann, R. J. Watson, and M. A. Doblin, *Mar. Chem.*, 2014, DOI: 10.1016/j.marchem.2014.10.002.

65. L. M. Laglera and C. M. G. van den Berg, *Limnol. Oceanogr.*, 2009, **54**, 610–619.

66. R. Yang and C. M. G. van den Berg, *Environ. Sci. Technol.*, 2009, **43**, 7192–7.

67. S. Batchelli, F. L. L. Muller, K.C. Chang, and C. Lee, *Environ. Sci. Technol.*, 2010, **44**, 8485–90.

68. L. M. Laglera, G. Battaglia, and C. M. G. van den Berg, *Mar. Chem.*, 2011, **127**, 134–143.

69. K. Misumi, K. Lindsay, J. K. Moore, S. C. Doney, D. Tsumune, and Y. Yoshida, *Global Biogeochem. Cycles*, 2013, **27**, 450–462.

70. R. M. Bundy, H. A. N. Abdulla, P. G. Hatcher, D. V. Biller, K. N. Buck, and K. A. Barbeau, *Mar. Chem.*, 2014, DOI: 10.1016/j.marchem.2014.11.005.